MENU 2007
11th International Conference
on Meson-Nucleon Physics and
the Structure of the Nucleon
September10-14, 2007
IKP, Forschungzentrum Jülich, Germany

Studies of the $\Lambda(1405)$ in Proton-Proton Collisions with ANKE at COSY-Jülich

I. Zychor

The Andrzej Sołtan Institute for Nuclear Studies
05-400 Świerk, Poland

Abstract

The lineshape of the $\Lambda(1405)$ was studied in the $pp \rightarrow pK^+Y^0$ reaction at a beam momentum of $3.65\,\mathrm{GeV/c}$ at COSY-Jülich. The ANKE spectrometer was used to identify two protons, one positively charged kaon, and one negatively charged pion in the final state. Invariant–mass and missing–mass techniques were applied to separate two neighbouring neutral excited hyperon resonances, the $\Sigma^0(1385)$ and $\Lambda(1405)$. Both the shape and the position of the $\Lambda(1405)$ distribution are similar to those measured in other reactions and this information contributes to the ongoing debate regarding the structure of this resonance.

1 Introduction

The $\Lambda(1405)$ is a well established four–star resonance [1] but it is still not well understood as a baryonic state; it does not fit in easily within the simple quark picture [2]. The $\Lambda(1405)$ might be the spin-multiplet partner of the $J^P = \frac{3}{2}^-$ $\Lambda(1520)$, a meson–baryon resonance, a $\overline{K}N$ quasibound state [3], or a $q^4\overline{q}$ pentaquark state [4]. Recent theoretical investigations based on chiral dynamics predict the existence of two poles in the vicinity of the $\Lambda(1405)$ [5–7] with a decay spectrum that depends upon the production process. In any event, the $\Lambda(1405)$ does not have a Breit–Wigner shape because of the opening at $1432\,\mathrm{MeV/c^2}$ of the decay mode $\overline{K}N$ [8–10]. Independent of the model, if the $\Lambda(1405)$ were a single quantum state, its lineshape should be independent of the method of production.

The $\Sigma^0(1385)$ and $\Lambda(1405)$ resonances overlap significantly because their widths of $36\,\mathrm{MeV/c^2}$ and $50\,\mathrm{MeV/c^2}$, respectively, are much larger than the mass difference of $\sim 20\,\mathrm{MeV/c^2}$. This is the main experimental difficulty in investigating the $\Lambda(1405)$ nature *via* the $\Sigma^+\pi^-$ and $\Sigma^-\pi^+$ decay modes since these are also possible final states for the $\Sigma^0(1385)$ disintegration. However,

the $\Lambda(1405) \to \Sigma^0 \pi^0$ decay can be used to identify this resonance unambiguously because isospin forbids this mode for the $\Sigma^0(1385)$.

In Fig. 1 the simplified decay scheme of excited neutral resonances with masses below 1432 MeV/c^2 demonstrates the differences between $\Sigma^0(1385)$ and $\Lambda(1405)$ utilised in the present analysis.

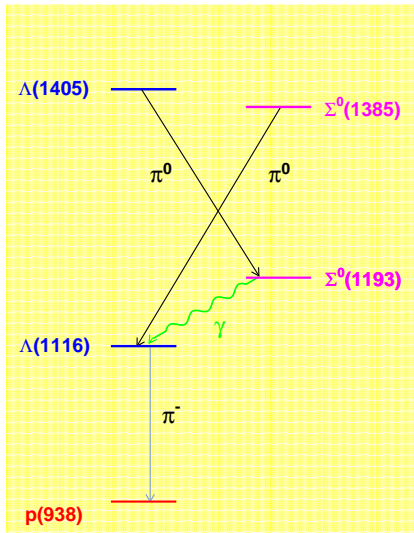Figure 1: Simplified decay scheme for the $\Lambda(1405)$ and $\Sigma^0(1385)$ hyperon resonances

2   Experiment, analysis and simulations

The experiment was performed at the Cooler Synchrotron COSY, a medium energy accelerator and storage ring for protons and deuterons, which is operated at the Research Center Jülich (Germany) [11]. COSY supplied a stored proton beam with a momentum of 3.65 GeV/c at a revolution frequency of $\sim 10^6\,\mathrm{s}^{-1}$. Using a hydrogen cluster–jet target, the average luminosity during the measurements was $L = (55 \pm 8)\,\mathrm{pb}^{-1}$.

The ANKE spectrometer [12] used in the experiments consists of three dipole magnets that guide the circulating COSY beam through a chicane. The central C–shaped spectrometer dipole D2, placed downstream of the target, separates the reaction products from the beam. The ANKE detection system, comprising range telescopes, scintillation counters and multi–wire proportional chambers, registers simultaneously positively and negatively charged particles and measures their momenta [13].

The following configuration of detectors was used to measure particles over a particular momentum range:

1. forward (Fd) and side–wall (Sd) counters for protons between $0.75\,\text{GeV/c}$ and the kinematic limit,

2. telescopes and side–wall scintillators for K^+ between 0.2 and $0.9\,\text{GeV/c}$,

3. scintillators for π^- between 0.2 and $1.0\,\text{GeV/c}$.

The angular acceptance of the spectrometer dipole D2 is $|\vartheta_\text{H}| \lesssim 12°$ horizontally and $|\vartheta_\text{V}| \lesssim 5°$ vertically. Momenta, reconstructed from tracks in multi–wire proportional chambers, allow the masses of particles to be determined to within $\sim 10\,\text{MeV/c}^2$.

A multiparticle final state, containing two protons, a positively charged kaon, a negatively charged pion and an unidentified residue X^0 selected the $pp \to pK^+p\pi^-X^0$ reaction. In the $\Sigma^0(1385) \to \Lambda\pi^0$ decay the X^0 residue is a π^0 while, for the $\Lambda(1405) \to \Sigma^0\pi^0$ decay, $X^0 = \pi^0\gamma$ (see Fig. 1).
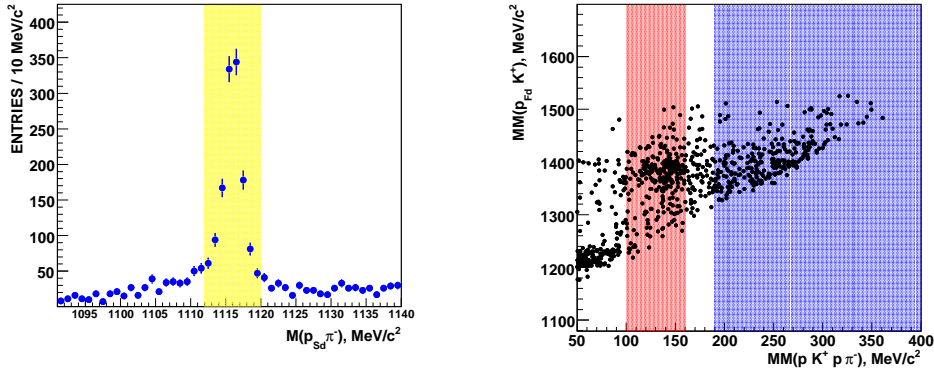

Figure 2: *Left:* Invariant mass $M(p_{Sd}\pi^-)$ measured in the $3.65\,\text{GeV/c}$ $pp \to pK^+\overline{Y^0}$ reaction. The yellow horizontal box shows the band used to select the Λ. *Right:* Missing mass $MM(p_{Fd}K^+)$ *versus* the missing mass $MM(pK^+\pi^-p)$. The left (red) vertical box covers the π^0 region and the right (blue) one has $MM(pK^+\pi^-p) > 190\,\text{MeV/c}^2 \gg m(\pi^0)$.

The following method was used to separate the $\Lambda(1405)$ from the $\Sigma^0(1385)$:

1. identify four particles: p_{Fd}, p_{Sd}, K^+ and π^-,

2. analyse events with the invariant mass of the $p_{Sd}\pi^-$ pair equal to the mass of the Λ,

3. select events with the missing mass of $(p_{Fd}, p_{Sd}, K^+, \pi^-)$ equal to a π^0 mass to isolate the $\Sigma^0(1385)$ and much higher than the π^0 mass to identify the $\Lambda(1405)$.

In the left part of Fig. 2 the invariant mass $M(p_{Sd}\pi^-)$ of the $p_{Sd}\pi^-$ pairs is shown, where the protons were registered in the side-detector counters. In the mass region around $1116\,\mathrm{MeV/c^2}$ a peak with a FWHM of $\sim 5\,\mathrm{MeV/c^2}$ is visible on a background that is mostly combinatorial in nature. The vertical box marks invariant–masses between 1112 and $1120\,\mathrm{MeV/c^2}$. Events within this box are plotted in the right panel of Fig. 2 in a distribution of $MM(p_{Fd}K^+)$ *versus* $MM(pK^+\pi^-p)$. The two vertical bands show the four–particle missing–mass $MM(pK^+\pi^-p)$ criteria used to separate the $\Sigma^0(1385)$ candidates from those of the $\Lambda(1405)$. The left band is optimised to identify a π^0 whereas the right one selects masses significantly greater than $m(\pi^0)$. The deviation of $\sim 8\,\mathrm{MeV/c^2}$ from the nominal pion mass of $135\,\mathrm{MeV/c^2}$ is not unexpected in a mass reconstruction involving four particles.
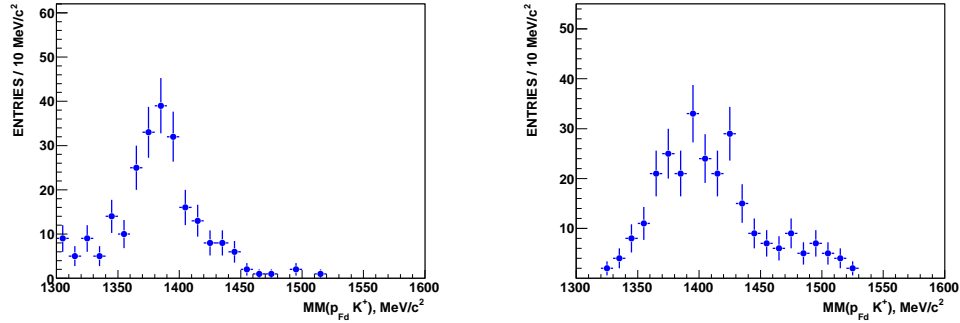

Figure 3: Missing–mass $MM(p_{Fd}K^+)$ distribution for the $pp \to pK^+p\pi^-X^0$ reaction for events with $M(p_{Sd}\pi^-) \approx m(\Lambda)$. The distribution obtained for $MM(pK^+\pi^-p) \approx m(\pi^0)$ is presented in the left panel and for $MM(pK^+\pi^-p) > 190\,\mathrm{MeV/c^2}$ in the right one.

In the left part of Fig. 3 the missing–mass $MM(p_{Fd}K^+)$ distribution is shown for $MM(pK^+\pi^-p) \approx m(\pi^0)$. A peak around a mass of $1385\,\mathrm{MeV/c^2}$ and a width of $\sim 50\,\mathrm{MeV/c^2}$ is seen on a rather small background. In the right part of Fig. 3 the distribution, obtained for $MM(pK^+\pi^-p) > 190\,\mathrm{MeV/c^2}$, has a peak near $1400\,\mathrm{MeV/c^2}$ and a tail on the high missing–mass side.

In order to explain the measured spectra, Monte Carlo simulations were performed to estimate backgrounds from non–resonant and resonant reactions. The following non–resonant processes have been included:
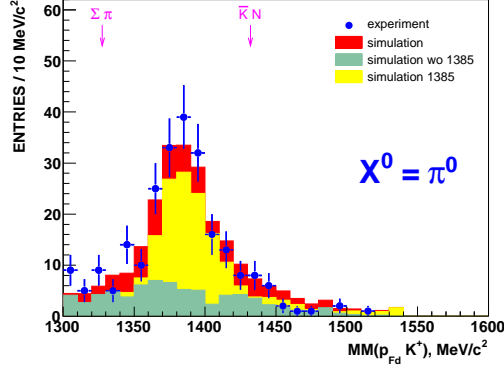
Figure 4: Missing–mass $MM(p_{Fd}K^+)$ distribution for the $pp \to pK^+p\pi^- X^0$ reaction for events with $M(p_{Sd}\pi^-) \approx m(\Lambda)$ and $MM(pK^+\pi^-p) \approx m(\pi^0)$. Experimental points with statistical errors are compared to the red histogram of the fitted overall Monte Carlo simulations. The simulation includes resonant contributions (yellow) and non–resonant phase–space production (green). Arrows indicate the $\Sigma\pi$ and $\overline{K}N$ thresholds.

1. $pp \to NK^+\pi X(\gamma)$

2. $pp \to NK^+\pi\pi X(\gamma)$

with X representing any allowed Λ or Σ hyperon. The second group consists of the following exclusive hyperon production reactions:

1. $pp \to pK^+\Sigma^0(1385)$

2. $pp \to pK^+\Lambda(1405)$

3. $pp \to pK^+\Lambda(1520)$

The simulations, based on the GEANT3 package, were performed in a similar manner to those in Ref. [14].

In the study of $\Sigma^0(1385)$ production and its backgrounds, events were generated according to phase space using a relativistic Breit–Wigner parameterisations for the known hyperon resonance [1]. The relative contributions of the resonant and non–resonant reactions were deduced by fitting the experimental data to the simulated spectra. In Fig. 4 the histograms show the resonant contribution from the $pp \to pK^+\Sigma^0(1385)$ reaction (solid-yellow) and the sum of non–resonant contributions (solid-green). The result of the overall simulations is shown as a red histogram.

Turning now to the $\Lambda(1405)$, simulations show that the $\Sigma^0(1385)$ does not contaminate the missing–mass $MM(pK^+\pi^-p)$ range above $190\,\mathrm{MeV/c^2}$ (see Fig. 5). This point is crucial since it allows us to obtain a clean separation of the $\Sigma^0(1385)$ from the $\Lambda(1405)$.
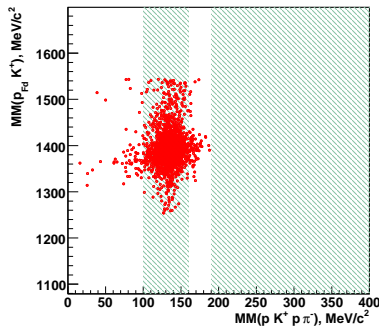

Figure 5: Simulated distribution of events with missing mass $MM(p_{Fd}K^+)$ *versus* $MM(pK^+\pi^-p)$. The left shaded vertical box covers the π^0 region and the right one has $MM(pK^+\pi^-p) > 190\,\mathrm{MeV/c^2} \gg m(\pi^0)$. Notice an absence of events in the right box.

In order to extract the $\Lambda(1405)$ distribution from the measured $\Sigma^0\pi^0$ decay, the non–resonant contributions have first been fitted to the experimental data. The resulting non–resonant background is indicated by the shaded histogram in the left panel of Fig. 6. When this is subtracted from the data, we obtain the distribution shown as experimental points in the right panel of Fig. 6.

3   Results

In Table 1 the information that is relevant for the evaluation of the total cross section is given. For both the hyperons measured this is of the order of a few μb.

The $(\Sigma\pi)^0$ invariant–mass distributions have been previously studied in two hydrogen bubble chamber experiments. Thomas *et al.* [10] found ~ 400 $\Sigma^+\pi^-$ or $\Sigma^-\pi^+$ events corresponding to the $\pi^-p \to K^0\Lambda(1405) \to K^0(\Sigma\pi)^0$ reaction at a beam momentum of $1.69\,\mathrm{GeV/c}$. Hemingway [8] used a $4.2\,\mathrm{GeV/c}$ kaon beam to investigate $K^-p \to \Sigma^+(1660)\pi^- \to \Lambda(1405)\pi^+\pi^- \to (\Sigma^+\pi^-)\pi^+\pi^-$ and measured 1106 events [8].

In Fig. 7 our experimental points are compared to the results of Thomas and Hemingway, which have been normalised by scaling their values down by
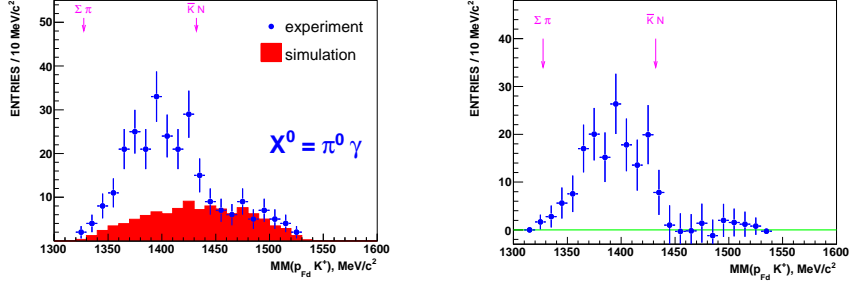
Figure 6: *Left:* Experimental missing–mass $MM(p_{Fd}K^+)$ distribution for the $pp \to \overline{pK^+p\pi^-X^0}$ reaction for events with $M(p_{Sd}\pi^-) \approx m(\Lambda)$ and $MM(pK^+\pi^-p) > 190\,\mathrm{MeV/c^2}$ compared to the shaded histogram of the fitted non–resonant Monte Carlo simulation. *Right:* The background–subtracted lineshape of the $\Lambda(1405)$ decaying into $\overline{\Sigma^0\pi^0}$.

factors of ~ 3 and ~ 7, respectively. The effect of the $\overline{K}N$ threshold is quite obvious in these data, with the $\Lambda(1405)$ mass distribution being strongly distorted by the opening of this channel. Despite the very different production mechanisms, the three distributions have consistent shapes.

This might suggest that, if there are two states present in this region, then the reaction mechanisms in the three cases are preferentially populating the same one. It should, however, be noted that by identifying a particular reaction mechanism, the proponents of the two–state solution can describe the shape of the distribution that we have found [7].

Table 1: Total cross section for the production of the $\Sigma^0(1385)$ and $\Lambda(1405)$ resonances in the $3.65\,\mathrm{GeV/c}$ $pp \to pK^+Y^0$ reaction

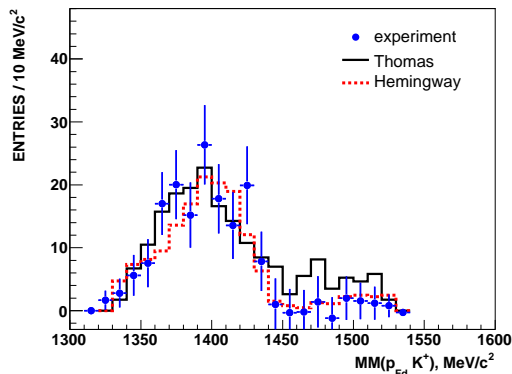|	$\Sigma^0(1385)$	$\Lambda(1405)$
number of events	170 ± 26	156 ± 23
acceptance	2.0×10^{-6}	4.4×10^{-6}
combined BR (%)	56	21
luminosity (pb^{-1})	55 ± 8	55 ± 8
detection efficiency (%)	55 ± 11	55 ± 11
cross section (μb)	$5.0 \pm 1.2_{\mathrm{stat}} \pm 2.0_{\mathrm{syst}}$	$5.6 \pm 0.8_{\mathrm{stat}} \pm 2.2_{\mathrm{syst}}$

Figure 7: The background–subtracted lineshape of the $\Lambda(1405)$ decaying into $\Sigma^0\pi^0$ (points) compared to $\pi^-p \to K^0(\Sigma\pi)^0$ [10] (black–solid line) and $K^-p \to \pi^+\pi^-\Sigma^+\pi^-$ [8] (red–dotted line) data.

4 Outlook

The decay of excited hyperons Y^{0*} via $\Lambda\pi^0$ and $\Sigma^0\pi^0 \to \Lambda\gamma\pi^0$ can be detected directly in electromagnetic calorimeters by registering neutral particles, i.e. γ and/or π^0. Measurements of such channels are underway in γp reactions (CB/TAPS at ELSA [15], SPring−8/LEPS [16]) and are also planned in pp collisions with WASA at COSY [17].

Acknowledgments

References

[1] W.-M. Yao et al., J. Phys. G **33**, 1 (2006), but see also the minireview in D.E. Groom et al., Eur. Phys. J. C **15**, 1 (2000).

[2] N. Isgur and G. Karl, Phys. Rev. D **18**, 4187 (1978).

[3] R.H. Dalitz and S.F. Tuan, Ann. Phys. (N.Y.) **10**, 307 (1960).

[4] T. Inoue, arXiv:0708.2339 [hep-ph].

[5] D. Jido *et al.*, Nucl. Phys. A **725**, 181 (2003).

[6] V.K. Magas, E. Oset and A. Ramos, Phys. Rev. Lett. **95**, 052301 (2005).

[7] L.S. Geng and E. Oset, arXiv:0707.3343 [hep-ph].

[8] R.J. Hemingway, Nucl. Phys. B**253**, 742 (1984).

[9] R.H. Dalitz and A. Deloff, J. Phys. G **17**, 289 (1991).

[10] D.W. Thomas, *et al.*, Nucl. Phys. B **56**, 15 (1973).

[11] R. Maier, Nucl. Instr. Meth. A **390**, 1 (1997)

[12] S. Barsov *et al.*, Nucl. Instr. Meth. A **462**, 364 (2001).

[13] M. Büscher *et al.*, Nucl. Instr. Methods A **481**, 378 (2002

[14] I. Zychor *et al.*, Phys. Rev. Lett. **96**, 012002 (2006).

[15] H. Schmieden, ELSA Letter of Intent ELSA/4-2003.

[16] H. Fujimura, AIP Conf. Proc. **915**, 737 (2007).

[17] H.-H. Adam *et al.*, nucl-ex/0411038.

[18] I. Zychor *et al.*, arXiv:0705.1039 [nucl-ex]